Journal of Drug Delivery Science and Technology 72 (2022) 103359

Contents lists available at ScienceDirect

Journal of Drug Delivery Science and Technology

journal homepage: www.elsevier.com/locate/jddst

Optimised release of tetracycline hydrochloride from core-sheath fibres produced by pressurised gyration

Hamta Majd [a], Anthony Harker [c], Mohan Edirisinghe [a], Maryam Parhizkar [b,*]

[a] Department of Mechanical Engineering, University College London, London, WC1E 7JE, UK
[b] School of Pharmacy, University College London, London, WC1N 1AX, UK
[c] Department of Physics and Astronomy, University College London, London, WC1E 6BT, UK

ARTICLE INFO

Keywords:
Core-sheath
Polymer
Pressurised gyration
Fibre
Drug delivery
Wound healing

ABSTRACT

In recent years, there has been a surge of interest in the design, processing, and use of core-sheath fibres, especially in the production of wound healing bandages and drug delivery. In this research, a novel core-sheath pressurised gyration technique was utilised to create antibacterial fibre patches (tetracycline hydrochloride, TEHCL) using polyvinyl pyrrolidone (PVP) and polycaprolactone (PCL). Antibiotic patches showed uniform fibres with a porous surface giving rise to a biphasic delivery system, which provided an initial burst of 30–48% drug release in the first 24 h followed by a constant rate of release throughout the course of 168 h, suitable for wound-dressings application. The effect of operating parameters on fibre morphology, the influence of the core-sheath structure and drug loading as well as a mathematical modelling was investigated and analysed. Fourier-transform infrared spectroscopy, and differential scanning calorimetry results demonstrated successful TEHCL encapsulation as well as the presence of both polymers in the core-sheath fibres. The surface morphology of the fibres was studied using scanning electron microscopy and the core-sheath structure was verified using confocal scanning microscopy. Therefore, the core-sheath pressurised gyration method offers an exciting chance to customise fibre patches in a hybrid polymeric system. These advancements are crucial in the world of healthcare to meet demands where antibacterial dressings cannot be produced rapidly or when a personalised approach is necessary.

1. Introduction

The management of wounds exerts a significant strain on healthcare resources [1]. There are many available options for wound dressings varying from basic gauze to complex dressings with various absorptive characteristics including foams, hydrocolloids, and alginates [2–4]. Although there are many dressing products available on the market, there is not enough evidence to support the effectiveness of these products [5]. Generally, antibacterial dressings are more expensive to purchase [6]. A study that was carried out in 2019 on the use of antibacterial wound dressings in England suggested a rise of over £28 million in expenditure between 1997 and 2016 [7].

Technological advancements in wound dressing, various chronic diseases, accident cases and the increase in the size of the elderly population, who are more prone to injuries, due to lack of cell multiplication are expected to fuel the market during the forecasted years [8,9]. However, concerns about the high costs associated with antibacterial wound dressings, which eventually raises the overall treatment costs to the patients, are anticipated to prevent the market growth. Through the years, researchers have carried out significant work on the production of both synthetic and natural antibacterial dressings. Nevertheless, there is still a huge gap in the market for antibacterial dressings that can be made on a large scale at a low cost.

Antibacterial dressings are vital in the treatment and prevention of soft tissue and skin infections during wound care [10]. They are used to protect wounds from infections and pathogens that can worsen the wound, leading to increased cost of treatment [11]. Antibacterial dressings can be used to treat acute wounds like abrasions, lacerations, cuts, and burns. They are also used for chronic wounds like surgical wounds, leg ulcers and pressure ulcers [12].

Injuries that break and damage the body tissues or the skin traverse through a wound healing process. An ordinary wound healing process is achieved in the human body through four accurate stages: haemostasis, inflammation, proliferation, and remodelling [13]. Nevertheless, the

* Corresponding author.
E-mail address: maryam.parhizkar@ucl.ac.uk (M. Parhizkar).

https://doi.org/10.1016/j.jddst.2022.103359
Received 5 February 2022; Received in revised form 18 April 2022; Accepted 20 April 2022
Available online 4 May 2022

process of wound healing can be detained by numerous systemic and local factors such as body type, age, chronic disease, hormones and infection that results in impaired tissue repair [14,15].

The effectiveness of these antibacterial wound dressings depends on their mechanical properties and drug delivery system. Fibres are very popular in the world of healthcare applications. This is owing to their distinct characteristics, which include a high surface area to volume ratio [16,17]. In order to produce fibres, a vast range of natural and synthetic polymers can be used [18]. Polymeric fibres can be made in several different forms, such as porous-surface, core-sheath, multilayer, side-by-side and hollow structures [19–23]. All these different structures are incredibly beneficial in a broad spectrum of modern applications, including filtration, wound healing, tissue engineering, and drug delivery systems [24]. There have been many different fibre production methods that have been used in both research and industrial settings [25]. The polymer material properties and the end application of the fibres will determine the suitable method of production [26]. There are numerous techniques such as coaxial electrospinning, coaxial wet-spinning, coaxial centrifugal spinning, coaxial solution blowing, and novel core-sheath pressurised gyration that have been developed for the formation of core-sheath fibres [27–30].

Coaxial electrospinning is perhaps the most often used manufacturing process to produce core-sheath fibres, in comparison to other methods due to its versatility and easy to use aspect. However, this technique's versatility is arguable due to its distinct limitations such as the use of high voltage, material selection, the requirement for specialised equipment, electrically conductive targets, and low yield [31–33].

Novel core-sheath pressurised gyration technique is an electric field-free manufacturing process that produces core-sheath structure fibres with two different polymers [34]. This fibre spinning method operates by loading the polymer solutions into a specially designed rotating vessel which forces the solution to be extruded via concentric nozzles as a result of combining pressure and rotational force [35]. This method has several advantages, one of which is the outstanding ability to mass-produce core-sheath polymeric fibres [36].

Throughout the years, numerous adjustments and remodelling have been applied to various spinning techniques to fabricate more advanced fibre structures with superior performances [37]. Fibres with core-sheath structures are considered to be some of the most advanced forms of fibres [38], due to their superior mechanical properties for healthcare applications [39]. The structure of these fibres consists of two layers of polymeric fibres, where the sheath polymer with a particular characteristic surrounds the core polymer, therefore, capitalising from unique features of both polymers [40].

Core-sheath fibres have a strong resemblance to the extracellular matrix, which can support the enhancement of cell adhesion, migration and proliferation making them suitable candidates for wound healing, tissue engineering and antimicrobial filtration [41]. Whilst core-sheath fibres can be used in many healthcare applications, research has shown their remarkable benefits in drug delivery systems, as having a shell coating on the fibres will adequately control the release profile of the drugs encapsulated in the core of the fibres [42]. In addition, core-sheath fibres have the ability to load more than one drug in the same fibre where their release rate can be regulated, leading to a better therapeutic effect whilst reducing toxicity [43].

Typically, in a single-liquid fibre spinning process, a slow dissolving or hydrophobic polymer is used to extend the time of the drug release from a polymeric fibre. Nevertheless, a huge setback is that a significant proportion of the incorporated drug is found at the fibre surface [44], which typically leads to a burst release (where a high amount of the drug is released immediately followed by a decrease in the rate of release) [45]. Consequently, this becomes a significant problem if modified release systems are required. Core-sheath structures provide one feasible approach to this problem by creating a two-compartment fibre, with the sheath consisting of a protective polymer layer whilst the drug is only encapsulated in the core of the fibre. However, to ensure the desired fibres are generated, careful study of the polymer selection, solvent and enhancement of the interface compatibility are crucial [46].

Polycaprolactone (PCL) is an excellent hydrophobic polymer used in a multitude of biomedical applications, attributing to its biodegradability, biocompatibility, chemical and thermal stability as well as significant mechanical and physical properties [47]. PCL polymer has shown much promise in tissue engineering and drug delivery systems because of its porous surface morphology which can act as a blueprint for cell adhesion, growth and differentiation as well as controlled release for wound dressing materials [48]. Polyvinylpyrrolidone (PVP) is a hydrophilic polymer that is identified for its adhesion features, complexion, physiological compatibility, and little chemical toxicity that can be used in drug delivery systems for fast-dissolving drug matrices [49]. Tetracycline hydrochloride (TEHCL) is a popular antibiotic with antimicrobial and anti-inflammatory properties which works by slowing down the growth of bacteria that can cause infection and reduce swelling [50]. TEHCL is often prescribed as a higher dose in the initial stage of the treatment to prevent infection and then tapered down to a lower dose to control the infection. Additionally, the incorporation of TEHCL could encourage the regeneration of fibroblasts to promote adequate wound healing by modulating its release from the core-sheath fibres [51].

In this study, novel core-sheath antibacterial fibre patches loaded with the drug were produced using the core-sheath pressurised gyration. The aim was to design a biphasic delivery system in a novel core-sheath structure that would release the drug at two different periods of time (burst/sustained), which provides an initial burst of drug followed by a steady rate of release over a defined period, suitable for wound-dressing applications. Therefore, in this work, core-sheath antibacterial fibres containing polycaprolactone (PCL), polyvinyl pyrrolidone (PVP) and tetracycline hydrochloride (TEHCL) were prepared. Four samples were tested for drug release analysis to show a more effective drug delivery system that can be made via a novel mass production technique such as core-sheath pressurised gyration. Additionally, a comparison of release between core-sheath PCL:PVP(TEHCL) and PCL:TEHCL fibres was carried out over a 168-h period in-vitro (Fig. 1). The drug was embedded in a hydrophilic polymer (PVP) as the core of the fibre and surrounded by a hydrophobic polymer (PCL) as the sheath. The results obtained were then compared with the case when the drug was encapsulated in PCL fibres alone. Furthermore, to find the optimal manufacturing process two different pressures were applied during the fibre fabrication manufacturing and the effect of process parameters on fibre diameter and morphology were analysed.

2. Materials and methods

2.1. Materials

PVP powder (MW 1.3×10^6 g mol^{-1}), PCL pellets (MW 8×10^4 g mol^{-1}), Rhodamine B, Acriflavine hydrochloride, chloroform and ethanol were acquired from Sigma Aldrich, UK. TEHCL was obtained from TOKU-E (Bakerview Spur Bellingham, USA). Phosphate buffer saline (PBS, pH = 7.4) was purchased from Oxoid ThermoFischer, UK.

2.2. Solution preparation

Core-sheath fibres: The polymer solution for the core of the fibres involved dissolving PVP powder into ethanol to make a concentration of 10 wt %. The polymer solution prepared for the sheath layer of the fibres involved mixing PCL pellets into chloroform to make a concentration of 10 wt %. The PVP solution was then mixed with TEHCL drug at a concentration of 2 wt %. All solutions were magnetically stirred for 24 h at an ambient temperature of 19–23 °C.

PCL fibres: The polymer solution prepared involved mixing PCL pellets into chloroform to make a concentration of 10 wt %. The PCL solution was then mixed with TEHCL drug at a concentration of 2 wt %. It was then magnetically stirred for 24 h at an ambient temperature of 19–23 °C.

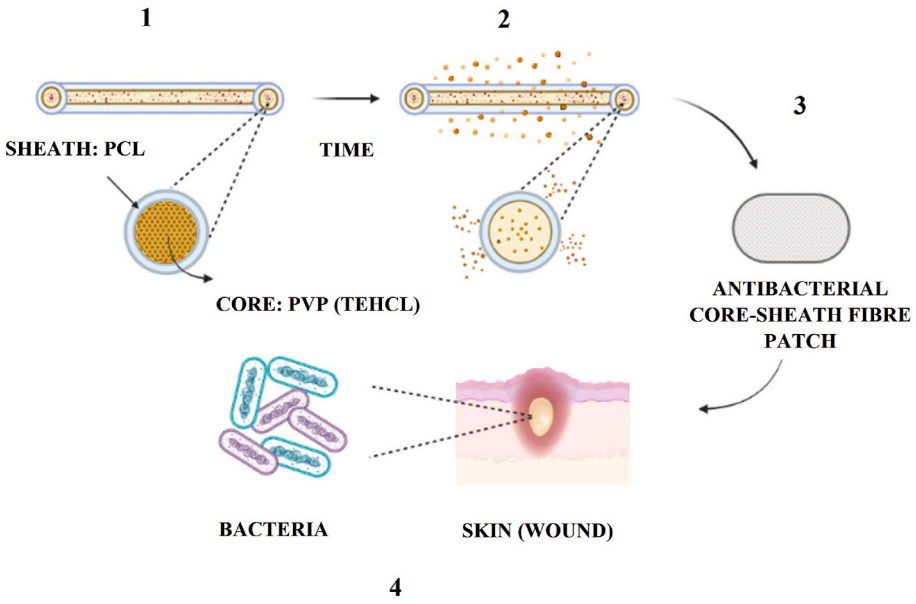

Fig. 1. Schematic view illustrating [1]: encapsulation of TEHCL drug in a core-sheath fibre structure [2], sustained release of the drug through the sheath of the fibre [3], final product: core-sheath antibacterial dressing [4], the use of the dressing for wound healing application.

2.3. Core-sheath pressurised gyration

The core-sheath pressurised gyration device shown in (Fig. 2) was used to fabricate core-sheath fibres. The equipment design consists of an aluminium twin-reservoir spherical pot with 100 mm outer diameter and 80 mm inner diameter. Both internal and external pot material volume capacity is 20 mL. Furthermore, the capillaries connected to the vessel have an external diameter of 1.6 mm and an internal diameter of 0.8 mm, additionally, once closed forms a total of 2 concentric orifices. The top of the vessel is attached to a pressurised gas (N_2) that can provide 0.1–0.3 MPa flow pressure. The bottom of the vessel is also attached to a DC motor which provides a maximum rotational speed of 6000 rpm. The polymer solutions were fed into the vessels through the inlet and outlet at the top of the vessel.

2.4. Fibre preparation

2.4.1. Core-sheath PCL:PVP(TEHCL)

The fabrication of core-sheath fibres involved loading a 3 mL volume of 10 wt % PVP (TEHCL) in the inner vessel to serve as the core of the fibres and a 3 mL volume of 10 wt % PCL in the outer vessel to serve as the sheath of the fibres. The solutions were spun for 60 s at two pressures (0.1 MPa and 0.2 MPa) and a constant rotational speed of 6000 rpm under ambient conditions (19.3 °C and 46–55% relative humidity) to form fibrous patches. The experiments were repeated three times. The centrifugal force which was created by the high speed of the rotation movement and flow pressure, pushed the polymer solutions through both capillaries of the vessel. Throughout this procedure, the solvent in the solution evaporates, resulting in the formation of a fibre patch.

2.4.2. PCL:TEHCL

The fabrication of PCL:TEHCL fibres involved loading a 3 mL volume of 10 wt % PCL:TEHCL in the inner vessel of the gyrator device and the outer vessel of the gyrator was left empty. The solution was spun for 60 s at two pressures (0.1 MPa and 0.2 MPa) and a constant rotational speed of 6000 rpm under ambient conditions (19.3 °C and 46–55% relative humidity) to form fibrous patches.

The experiments were performed in triplicate.

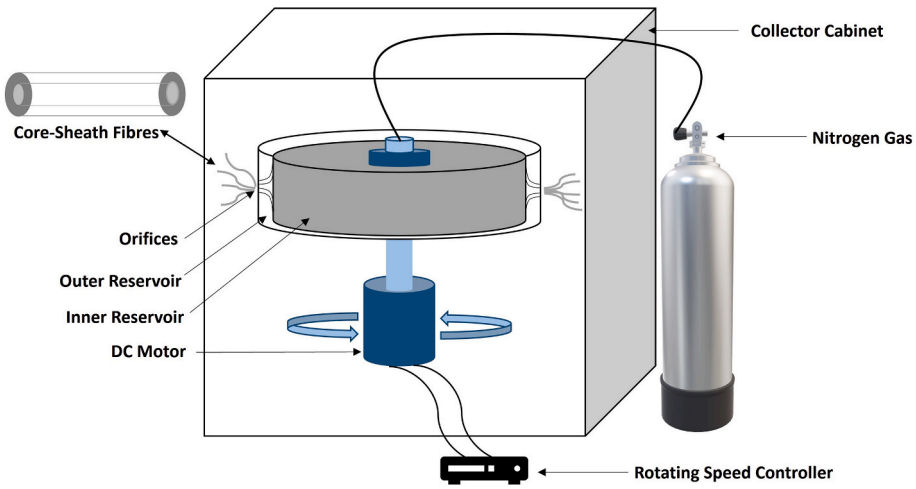

Fig. 2. Core-sheath pressurised gyration.

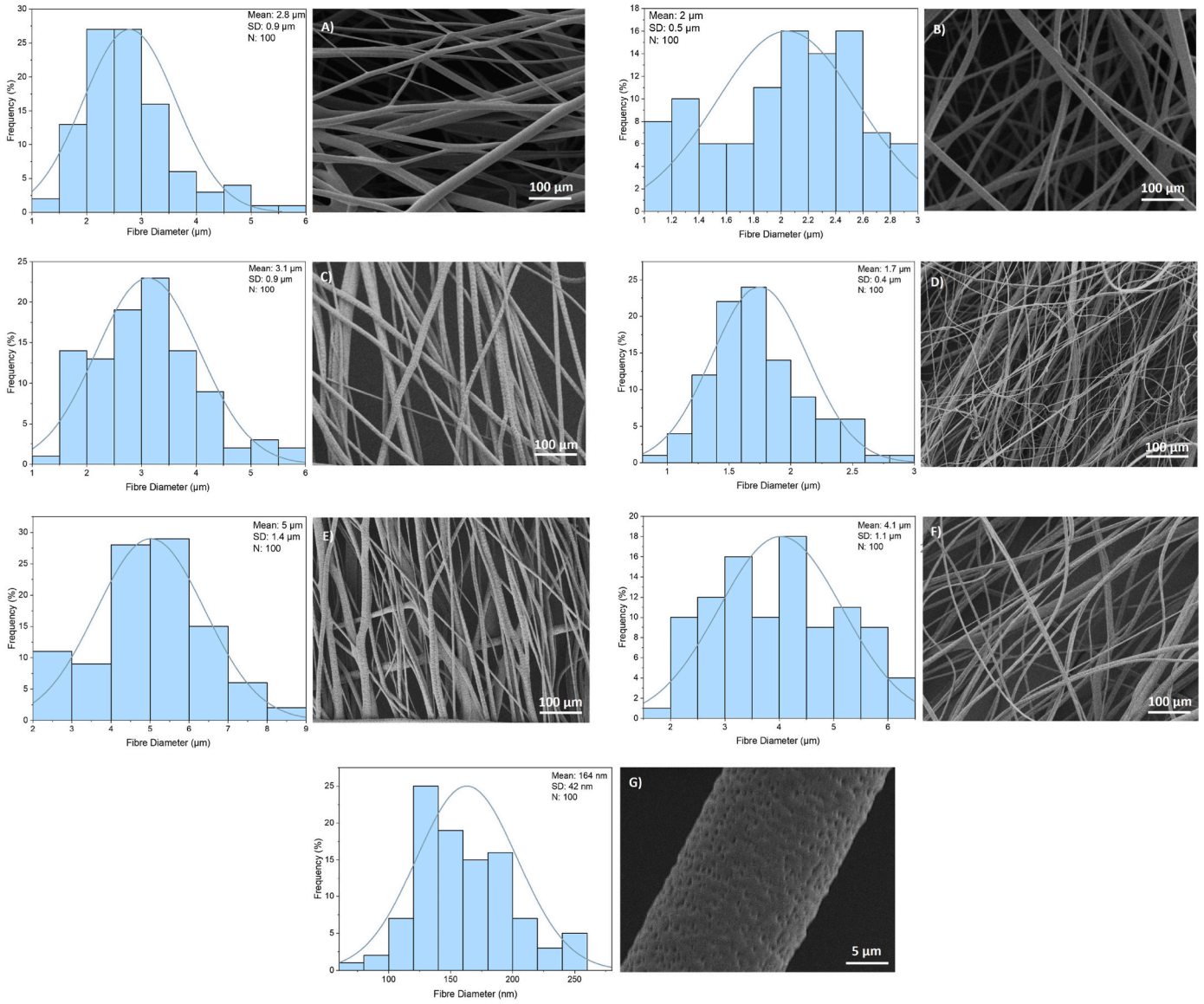

Fig. 3. SEM images and size distribution graphs of: A) PVP (0.1 MPa), B) PVP (0.2 MPa), C) PCL:PVP(TEHCL) (0.1 MPa), D) PCL:PVP(TEHCL) (0.2 MPa), E) PCL:TEHCL (0.1 MPa), F) PCL:TEHCL (0.2 MPa), G) PCL:PVP(TEHCL). The dips seen in the size distributions are not significant as established by the Hartigan's dip test and hence unimodal distributions are presented.

2.5. Fibre characterisation

2.5.1. Scanning electron microscopy (SEM)

The surface morphology of the PVP, Core-Sheath PCL:PVP(TEHCL) and PCL:TEHCL fibres were analysed using a scanning electron microscope (SEM) (Hitachi S-3400n) at an accelerating voltage of 5 kV. The surface of the samples was gold sputter-coated for 90 s using (Q150R ES, Quorum Technologies). The micrographs obtained from SEM imaging were analysed using Image J software to calculate the average fibre diameter and size distribution. For this study, 100 strands of fibres from each study were selected at random for size measurements. The average fibre diameter was calculated and plotted using Origin Pro software. A comparative analysis between two applied pressures (0.1 and 0.2 MPa) was carried out using the fibre diameter data.

2.5.2. Confocal microscopy (CM)

To observe the structure of the core-sheath fibres two different fluorescent dyes, rhodamine B (excitation at 543 nm) in the sheath and acriflavine hydrochloride (excitation at 490 nm) in the core were dissolved at a concentration of 1 wt % into the respective PCL and PVP solutions. The spun fibre samples were collected on a glass slide for imaging using confocal microscopy (Zeiss LSM 710) and the fluorescence of the fibres was studied using a 10 x oil immersion objective. The images captured were then analysed using ZEN 2012 software.

2.5.3. Differential scanning calorimetry (DSC)

The change in physical properties of PCL:PVP:TEHCL physical mix, PCL:TEHCL, PVP, Core-Sheath PCL:PVP:TEHCL fibres and pure TEHCL samples was determined by using (DSC Q2000) device and (TA Instrument) software. Prior to the measurements, 5 mg of each sample were positioned in aluminium DSC pans, hermetically sealed, and heated from 0 to 250 °C at a rate of 10 °C/min under a 50 mL/min gas flow (N_2).

2.5.4. Fourier transform infrared spectroscopy (FTIR)

The interaction between the drug, polymers and chemical reaction within the produced fibres were analysed using FTIR spectroscopy (PerkinElmer Spectrum 100). Prior to the measurement, 2 mg of each sample (PCL, PVP, Core-Sheath PCL:PVP, TEHCL, PCL:TEHCL, Core-Sheath PCL:

PVP(TEHCL)) were positioned on the ATR crystal and studied over 10 rounds in the range of 4000–500 cm^{-1} at a resolution of 4 cm^{-1}.

2.5.5. Loading of TEHCL and in-vitro release study

Encapsulation Efficiency (EE) of TEHCL investigation were carried out by dissolving 20 mg of both core-sheath and PCL fibres in chloroform. The concentration of TEHCL in chloroform was then determined using Cary UV–Vis spectroscopy at 363 nm.

Furthermore, PBS (pH = 7.4) was employed as the test medium for in-vitro TEHCL release testing of core-sheath and PCL fibres. The concentration of TEHCL in PBS was determined using UV–Vis spectroscopy at 363 nm. Preliminary to the release experiment, a linear calibration curve was created using a series of standard solutions with concentrations ranging from 5 to 40 g/mL. The release study was carried out by placing 20 mg of drug-loaded core-sheath and PCL fibrous patches into a 10 mL test medium, incubated in a shaker at 37 °C. Moreover, at 2, 4, 6, 8, 24, 48, 72, 96, 120, 144 and 168 h predetermined intervals, 2 mL of supernatant from each assessment media was removed and restored with 2 mL of new test medium to maintain sink condition. The removed supernatant was filtered using a 0.45 μm Millipore and analysed using a UV spectrophotometer. Obtained data collected was used to calculate the cumulative release percentage. The experiments were carried out in triplicate.

2.5.6. Mathematical modelling

The model for diffusive release from a cylinder with immediate transport of the dissolved diffusing species away from the surface is covered in detail by Crank where the underlying assumption is that the concentration outside the cylinder is zero [52].

In the case of a cylinder of radius b, in which the initial concentration is c_0 in $0 < r \leq a$ and c_1 in $a < r \leq b$ and the diffusion coefficient is D, the release fraction can be conveniently expressed in terms of $\chi = c_0/c_1$, $\rho = a/b$ and a scaled time $\tau = Dt/b^2$ as:

$$\varphi(\tau) = 1 - \sum_{n=1}^{\infty} \frac{4}{1 + \rho^2 + (\chi - 1)} e^{-\tau\beta_n^2} \frac{1}{\beta_n^2} \left[1 - (1 - \chi)\rho \frac{J_1(\rho\beta_n)}{J_1(\beta_n)} \right]$$

where the β_n are the solutions of:

$$Jo(\beta_n) = 0$$

and J_0 and J_1 are the Bessel functions of the first kind of order 0 and 1.

A further development of the model allows for concentrations c_0 in $0 < r \leq \rho b$, c_1 in $\rho b < r \leq \sigma b$ and c_2 in $\sigma b < r \leq b$, in which case the fractional release is:

$$\varphi(\tau) = 1 - \sum_{n=1}^{\infty} \frac{4}{1 + \rho^2 + (\chi - \varepsilon) + \sigma^2(\varepsilon - 1)} e^{-\tau\beta_n^2} \frac{1}{\beta_n^2} \left[1 + (\chi - \varepsilon)\rho \frac{J_1(\rho\beta_n)}{J_1(\beta_n)} + (\varepsilon - 1)\sigma \frac{J_1(\sigma\beta_n)}{J_1(\beta_n)} \right]$$

where the βn are as before, and $\chi = c_0/c_2$, $\xi = c_1/c_2$. This is applicable to a core-sheath structure with different initial concentrations in the core and sheath as well as an extra surface layer, but with the assumption of equal diffusion coefficients in the core and sheath [53].

It was also important to consider how distribution of the diffusing species might evolve during storage. Here the assumption was that diffusion may occur within the cylinder, but that no material leaves the cylinder. In this case, the concentration at a scaled radius $r = \sigma b$ at scaled time τ is given by:

$$\frac{c(\sigma, \tau)}{c_1} = 1 + (\chi - 1)\rho^2$$

$$+2 \sum_{n=1}^{\infty} e^{-\tau\infty_n^2} \frac{J_0(\sigma\infty_n)}{\infty_n J_0(\infty_n)^2} \rho(\chi - 1) J_1(\rho\infty_n)$$

where the α_n are the solutions of

$$J_1(\alpha_n) = 0$$

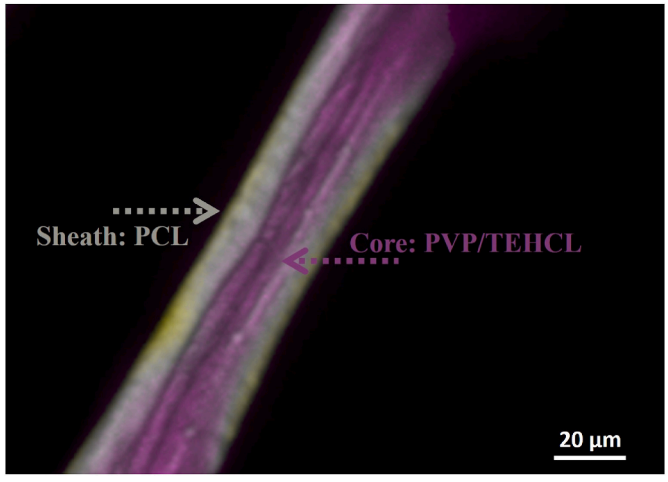

Fig. 4. Confocal microscopy image of core-sheath PCL:PVP(TEHCL) fibre, Rhodamine B (grey) illustrating the sheath and Acriflavine hydrochloride (purple) illustrating the core. (For interpretation of the references to colour in this figure legend, the reader is referred to the Web version of this article.)

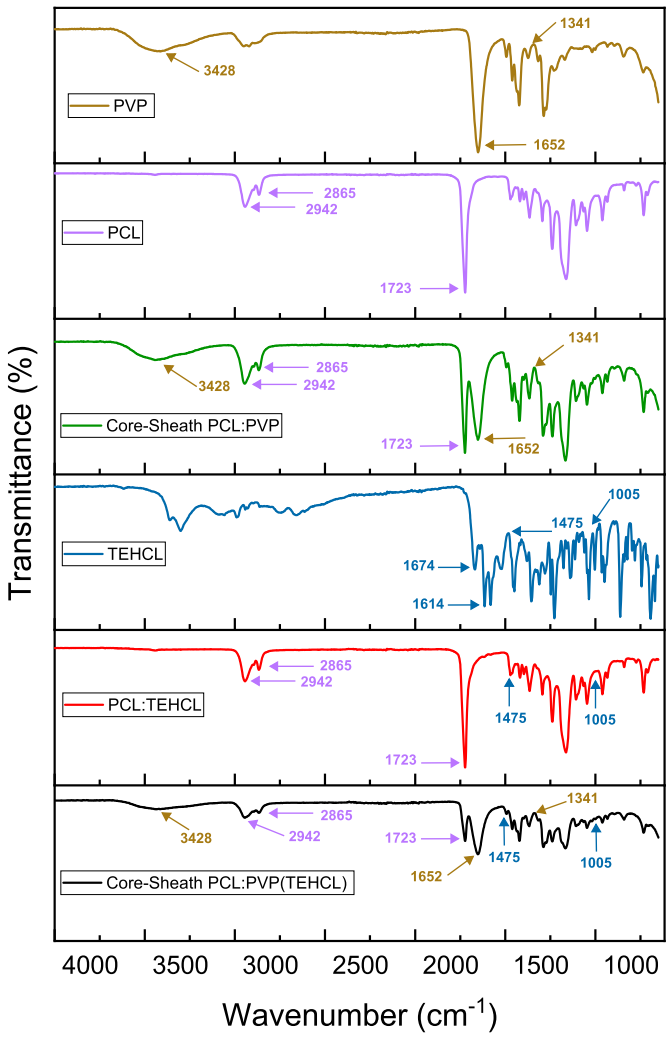

Fig. 5. FTIR spectra of fabricated fibres.

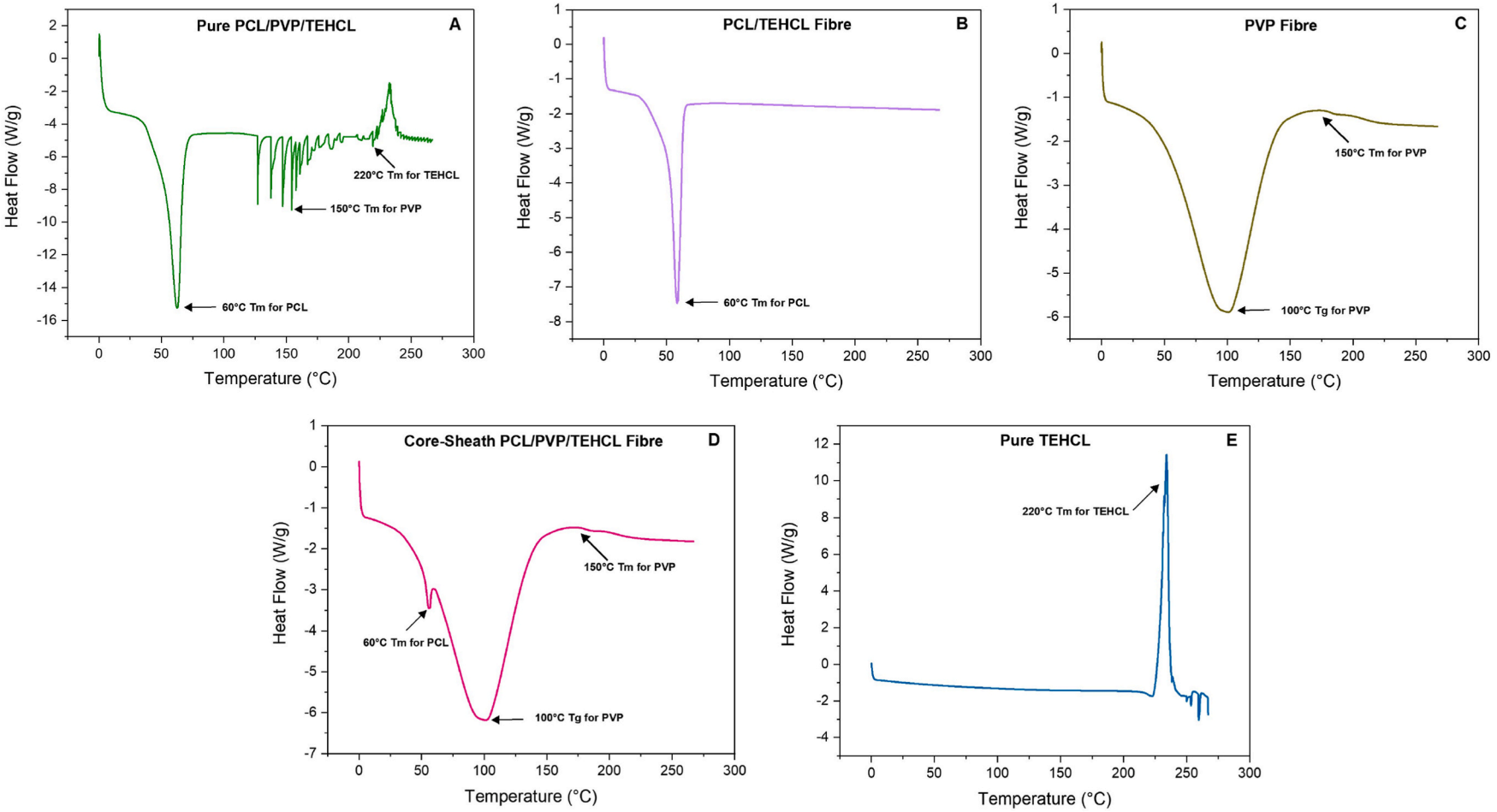

Fig. 6. DSC thermograms of: A) Pure PCL:PVP:TEHCL, B) PCL:TEHCL fibre, C) PVP fibre, D) PCL:PVP(TEHCL) fibre, E) Pure TEHCL.

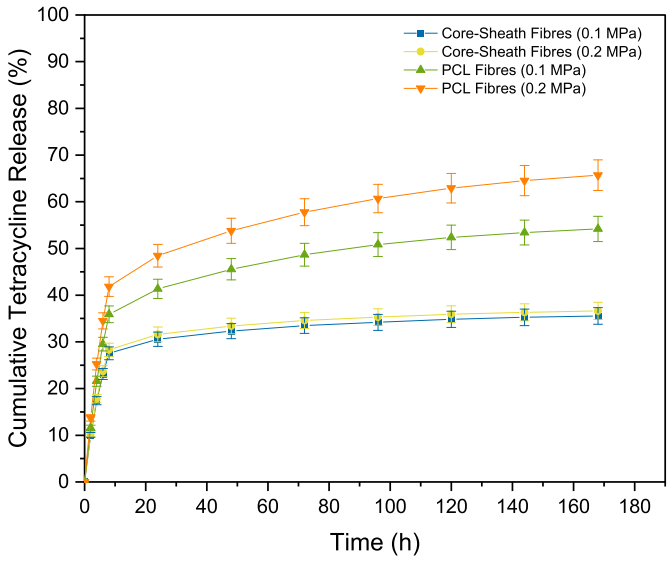

Fig. 7. TEHCL released from fibre patches of PCL:PVP(TEHCL) and PCL:TEHCL samples fabricated at 0.1 & 0.2 MPa.

In the results reported below, we have truncated the infinite sums over n at n = 100.

Finally, we considered the possibility of "burst release", assuming that a fraction f of the content of each fibre is available for immediate release and is dissolved at a rate governed by diffusion through a stagnant layer of fluid around the particle, whilst the remaining (1 − f) is released after diffusing through the solid particle. This results in a release:

$$\varphi(\tau) = \mathrm{fe}^{-\mathrm{kt}} + (1-\mathrm{f})\varphi_{sol}(\mathrm{t})$$

where $\varphi_{sol}(t)$ represents the release by solid-state diffusion [52].

3. Results and discussion

3.1. Scanning electron microscopy

Fig. 3 shows the scanning electron micrographs of PVP, PCL:TEHCL and Core-Sheath PCL:PVP(TEHCL) fibres fabricated at a working pressure of 0.1 MPa and 0.2 MPa at a constant rotational speed of 6000 rpm. PVP fibres fabricated at a working pressure of 0.1 MPa showed an average diameter of 2.8 μm ± 0.9 μm (Fig. 3A). The fibres had a smooth, bead-free surface and were well aligned. Additionally, PVP fibres obtained at 0.2 MPa had a mean diameter of 2 μm ± 0.5 μm (Fig. 3B). PCL: TEHCL fibres produced at 0.1 MPa had an average diameter of 3.1 μm ± 0.9 μm (Fig. 3C). Whereas the fibres produced at 0.2 MPa had an average diameter of 1.7 μm ± 0.4 μm (Fig. 3D). It is clear that an increase in the pressure applied leads to a decrease in the fibre diameter in comparison to the PCL: TEHCL fibres produced at 0.1 MPa. The surface morphology of the fibres was nano-porous which is a result of rapid solvent evaporation [54]. This can be a great advantage for a burst release drug delivery system. This is due to the fact that the pores on the fibre surface will control the amount of substances that can travel through the fibre patch and the diffusion rate across the fibre mat [55]. Therefore, the porosity of the fibre surface will influence the drug release profile observed, as discussed later. Furthermore, surface porosity of the fibre makes it suitable for wound dressing as their porosity enables them to soak any fluid released from the wound, while their interconnected form promotes cell growth [56].

Core-sheath PCL:PVP(TEHCL) were successfully produced using the combination of the two materials. The core-sheath fibres obtained at 0.1 MPa had an average diameter of 5 μm ± 1.4 μm (Fig. 3E). Higher pressure of 0.2 MPa applied decreased the fibre diameter in comparison to 0.1 MPa, as an average diameter of 4.1 μm ± 1.1 μm was shown (Fig. 3F). The surface of the core-sheath fibres was also nano-porous, and this is due to having PCL in the sheath and PVP in the core as the solvent used in the sheath of the fibre is a volatile compound (chloroform). This occurs as a result of chloroform rapidly evaporating which generates a temperature variation on the surface of the fibre. Additionally, it causes condensation of droplets that EC evaporarate and result in pores [54]. The average diameter of these nano-pores was 164 ± 42 nm (Fig. 3G). The pores can raise the useful surface area to volume ratio of the patches and facilitate for the natural flow exchange of fluid exiting the patches, which is a required feature of antibacterial dressings [57]. In addition, the pores on the fibre surface allow the drug to diffuse out easily, which can lead to a rapid burst release [58]. It is also concluded that as the applied pressure increases during fibre production, the diameter of the fibres decreases. This is due to the introduction of more air into the solution during the processing, accelerating the evaporation of solvent by diffusion of solvent out of polymers to the surface, leading to the production of thinner fibres. Furthermore, core-sheath fibres had an increase in fibre diameter in contrast with PCL:TEHCL and PVP.

3.2. Confocal microscopy

Confocal microscopy was used to visualise the structure of the core-sheath fibres. The images obtained, confirmed the presence of a core-sheath structure, where the sheath is homogeneously distributed across the core of the fibre as shown in (Fig. 4). The grey colour represents PCL in the sheath and the purple colour represents PVP:TEHCL in the core. The visual evidence of a core-sheath fibre produced by this novel electric field-free technique launches innovative opportunities for various hybrid polymeric systems in drug delivery and wound healing applications.

3.3. Fourier transform infrared spectroscopy

FTIR analysis was carried out to validate the existence of components and probable interactions between them in all of the fibre patches. Fig. 5 illustrates the FTIR absorbance of PVP, PCL, Core-Sheath PCL:PVP, TEHCL, PCL:TEHCL and Core-Sheath PCL:PVP(TEHCL) fibre patches. The PVP peaks at 1652 cm^{-1} confirmed the presence of asymmetric stretching of CH_2 and stretching of C–O. The C–H bending and CH_2 wagging occur at 1423 cm^{-1} and 1288 cm^{-1} [59]. The peaks at 1018 cm^{-1} and 568 cm^{-1} can be branded as the CH_2 rocking mode and N–C=O bending [60]. The PVP peaks displayed at 3428 cm^{-1}, 1652 cm^{-1} and 1341 cm^{-1} were also indicated in Core-Sheath PCL:PVP as well as Core-Sheath PCL:PVP(TEHCL).The sharp PCL peaks were the prominent C=O stretch at 1723 cm^{-1}, CH_2 (alkane) medium numerous ring stretch at 2942 cm^{-1} and at 2865 cm^{-1} [61] were also demonstrated in the Core-Sheath PCL:PVP, Core-Sheath PCL:PVP(TEHCL) and PCL:TEHCL patches. Characteristic peaks for TEHCL were indicated at 1674 cm^{-1} for C=O, 1614 cm^{-1} for C=C (conjugated alkene) stretching, 1475 cm^{-1} for C–C stretching of an aromatic ring, C–N stretching in the spectrum of 1250–1200 cm^{-1}, and two mild N–H stretching peaks (dominant amide) at 3300 cm^{-1} and 3361 cm^{-1} [62]. The TEHCL drug peaks present at 1475 cm^{-1} and 1005 cm^{-1} were also identified in the Core-Sheath PCL:PVP(TEHCL) and PCL:TEHCL patches. Therefore, the existence of the TEHCL drug in the fibre patches can be confirmed. Furthermore, the results indicate no chemical binding between the drug and the polymers have taken place and all their individual spectroscopy detected characteristics have remained the same.

3.4. Differential scanning calorimetry

DSC analysis was carried out to analyse the thermal properties: glass transition (T_g), crystallisation (T_c) and melting temperature (T_m) of the fibre patches along with miscibility, and the presence of both polymers in the core-sheath patches. Initially, a physical mix of pure PCL, PVP and TEHCL was used to analyse the raw materials thermal properties as

shown in (Fig. 6A). As illustrated in the DSC thermograms (Fig. 6B), an endothermic peak matching to the melting point of PCL:TEHCL fibres was indicated at 60 °C. Amorphous PVP fibres alone showed a broad endothermic transition at 100 °C (Fig. 6C) which is ascribed to its glass transition [63,64]. This is due to the hydroscopic nature of PVP and moisture build-up during the gyration process. The small curve around 150 °C is linked to its melting point, which is attributed to the molecular weight and concentration of the polymer as it is proven that higher MW and concentration affects the T_m, T_c and T_g of the fibres [65]. The core-sheath fibres DSC thermograms (Fig. 6D) confirmed the presence of PVP and PCL polymers as there are two endothermic peaks of 60 °C PCL and 100 °C PVP which were also present in PCL and PVP thermographs (Fig. 6B and C). Additionally, the same small curve at 150 °C can be seen which also appeared in PVP fibres alone. The absence of TEHCL in the drug loaded core-sheath and PCL fibres thermographs was due to the drug being molecularly dispersed within the polymeric fibres in an amorphous phase [66]. This can be the result of a rapid solvent evaporation during the gyration process, which inhibited TEHCL crystal formation. Moreover, pure TEHCL drug thermograms (Fig. 6E) revealed a sharp exothermic peak at 220 °C which is in close agreement with the thermal behaviour of TEHCL [67].

3.5. Loading of TEHCL and in-vitro release study

Core-sheath pressurised gyration process provides an efficient method to encapsulate bioactive substances inside nano to macro-scale fibres. Encapsulation efficiencies of the core-sheath PCL:PVP(TEHCL) fibres obtained at 0.1 MPa was 45% and 0.2 MPa was 51%. The PCL:TEHCL fibres generated at 0.1 MPa showed 60% encapsulation efficiencies and 66% at 0.2 MPa. It can be seen that the higher applied pressure for both samples showed promising results with higher encapsulation efficiencies.

The drug release profile of the core-sheath fibre patches has been examined in this study. Cumulative release of TEHCL from two different types of fibre patches (Core-sheath PCL:PVP(TEHCL) and PCL:TEHCL) made at two different applied pressures (0.1 and 0.2 MPa) were tested during a 168 h incubation period. All four patches showed an initial release of 10–13% in the first hour. However, there was a burst release of 30–48% in the first 24 h. This is a well-known behaviour of drug loaded fibres which is a result of drug accumulation on the fibre surface [51]. Nevertheless, the rate of release slowed down with a sustained release profile after 24 h. In the overall duration of 168 h, the core-sheath fibres obtained at 0.1 MPa had a maximum drug release of 35% and the fibres obtained at 0.2 MPa had a maximum release of 36%. Additionally the PCL:TEHCL fibres showed a higher release profile of 54% at 0.1 MPa and 65% at 0.2 MPa in the duration of 168 h. The trend of release was similar for all four patches. Furthermore, both patches also showed a higher release profile at a higher pressure of 0.2 MPa. In comparison the fibre structures PCL:TEHCL showed a faster release profile than PCL:PVP (TEHCL) fibres in the duration of 168 h (Fig. 7). From the results obtained it can be confirmed that the core-sheath structure produced from the core-sheath gyration technique allowed the drug to be encapsulated in a hydrophilic polymer (PVP) as the core has the protection of a hydrophobic polymer PCL as the sheath. This composition showed a similar release profile as the hydrophobic polymeric (PCL) fibre containing the drug alone, meaning that core-sheath pressurised gyration technique opens a vast opportunity of using hydrophilic polymers in a core-sheath structure to attain sustained drug delivery system. Lastly the study of core-sheath fibres showed an initial burst release which was then followed by a sustained release.

Even though it is usually preferable to minimise an initial burst release for a sustained drug delivery system, such rapid release in the initial stage of dissolution can be beneficial for wound healing applications [68]. This is because of the fact that it can offer a loading dose, promptly boosting the drug's blood plasma concentration into the therapeutic window [69]. Following a slow release, a therapeutic concentration can be preserved throughout a period of time [70]. It can be confirmed by this study that the prospective of only using a hydrophobic fibre shell in a core-sheath structure and a drug encapsulated core does not always prohibit a burst release. Another important factor is the control of the pressurised gyration parameters to maintain a minimum porosity of the sheath layer as the loaded drug can diffuse through the pores on the surface of the sheath layer. More pores lead to a much faster rate of diffusion and therefore a faster release rate. Although some biomedical applications necessitate highly porous surfaces, which can mimic the biological environment they tend to interact with, in order to improve biocompatibility [71].

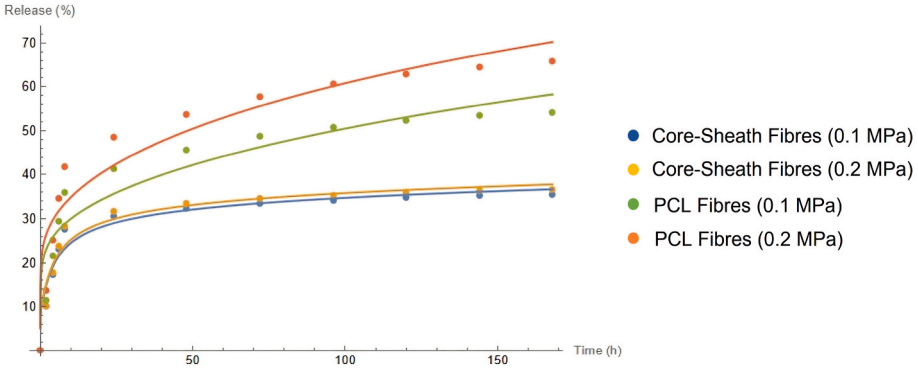

Fig. 8. The release percentage of TEHCL escaping from cylindrical fibres in the second series of experiments, showing the agreement of the experimental measurements (points) and the theoretical model (lines).

Table 1
Values of diffusion coefficient D and surface concentration factor $1/\chi$ deduced from fitting the model to the data from the second set of experiments. The uncertainties in D are caused by the uncertainties in the fibre diameters.

	Diameter μm	D $m^2 s^{-1}$	χ
Core-Sheath PCL:PVP(TEHCL) (0.1 MPa)	5.4 ± 1.4	$(1.3 \pm 0.7) \times 10^{-20}$	28
Core-Sheath PCL:PVP(TEHCL) (0.2 MPa)	4.7 ± 1.4	$(9 \pm 6) \times 10^{-21}$	30
PCL:TEHCL (0.1 MPa)	3.1 ± 1.1	$(3.3 \pm 1.9) \times 10^{-19}$	14
PCL:TEHCL (0.2 MPa)	1.5 ± 0.3	$(10 \pm 4) \times 10^{-20}$	15

3.6. Mathematical modelling

To account for the rapid release at early times from all the fibre formulations, initial calculations were made using a model in which the drug is initially uniformly distributed except for a higher concentration by a factor χ in the region outside 0.99 times the fibre radius. The diffusion coefficient D and the concentration factor χ were adjusted to obtain the best fit to the experimental release data, and the results are shown in (Fig. 8).

Using the measured fibre radii, it is possible to deduce the diffusion constant for the drug in the polymer, D. The results from the set of experiments, together with the values of χ, are given in Table 1. It is notable that the values of D and of χ are quite similar for PCL:PVP (TEHCL) obtained at 0.1 MPa and 0.2 MPa, with different values for PCL: TEHCL obtained at 0.1 MPa and 0.2 MPa.

The diffusion coefficients deduced for the core-sheath fibres with a PVP core are much less than those for the PCL:TEHCL fibres. The model assumed that the diffusion coefficients in the core and the sheath were equal and attempts to improve the fits using different core and sheath diffusions coefficients were inconclusive.

It is worth noting that the fibres were typically stored for about one day between production and release measurements. During this time, there could have been some diffusive redistribution of TEHCL within the core sheath fibres. Assuming a uniform diffusion coefficient, then the concentration profile in the core-sheath fibre assuming an initial non-zero concentration in the core and zero concentration in the sheath can be computed. Fig. 9 shows how the profile would evolve with a diffusion coefficient typical of the homogeneous fibres. With the much smaller diffusion coefficient, typical of the core-sheath fibres, a much slower evolution is expected of the concentration profile during storage, as shown in (Fig. 10). In this case the storage has little effect on the concentration profile.

An alternative approach is the explicit "burst release" model described above, and we have applied this to the experimental results. Fig. 11 shows the results of calculations when the drug is assumed to be uniformly distributed throughout the fibres in all cases, whereas (Fig. 12) is for the designed core-sheath distributions. The corresponding fitting parameters are given in Tables 2 and 3 respectively: there is very little difference in the quality of the fit between the uniform and core-sheath assumptions, but in all cases the "burst release" model fits the experiments better than the purely diffusive models. It is worth noting that the fraction of the loading associated with the burst release is very similar to the fraction which was included in the outer region of the fibres in our initial calculations and that quite similar drug diffusion coefficients are obtained in both models. Therefore, this model fits the experiments better than the purely diffusive models.

It can be noted that when the designed core-sheath drug concentration profile is assumed the burst release fraction is larger than for a uniform profile. This is to be expected and compensates for the delay in the drug in the core reaching the surface of the fibre.

4. Conclusions

For the first time, the core-sheath pressurised gyration technique has been used successfully to produce drug loaded antibacterial core-sheath fibres. The effect of manufacturing parameters on the fibre morphology was determined, leading to process optimisation. The results demonstrated that by applying a higher pressure, smaller fibre diameter was obtained and better encapsulation efficiency was shown. Antibacterial fibre patches were fabricated at micrometre-scale and with inter-fibrous pore size which led to a better biocompatibility as a wound dressing. Furthermore, characterisation data analysis of FTIR and DSC results

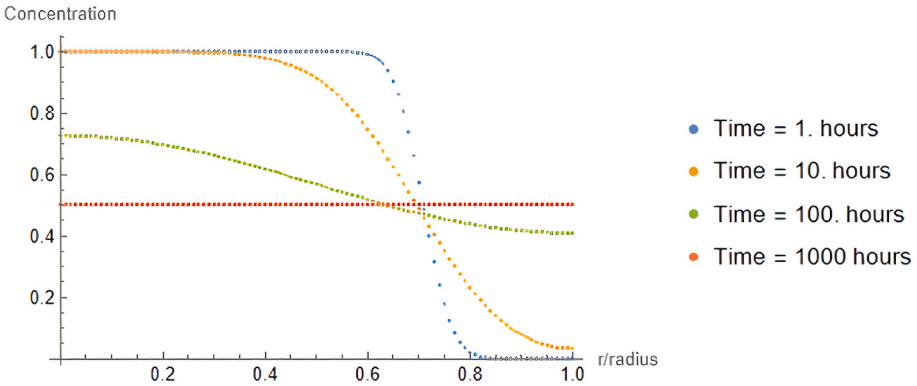

Fig. 9. Evolution of the concentration profile in a core-shell fibre with storage time, with a diffusion coefficient typical of those found for the homogeneous PCL fibres.

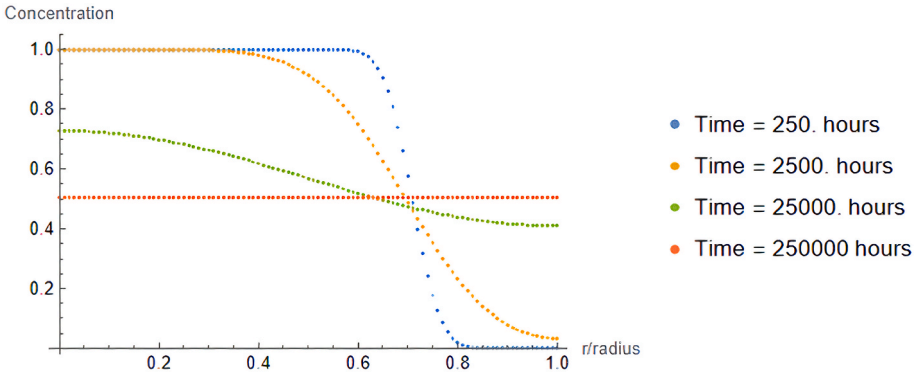

Fig. 10. Evolution of the concentration profile in a core-shell fibre with storage time, with a diffusion coefficient typical of those found for the PVP-PCL fibres.

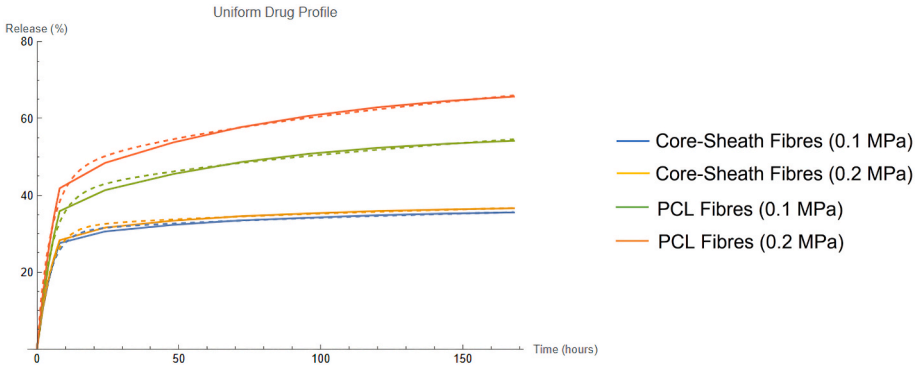

Fig. 11. The release percentage of TEHCL escaping from cylindrical fibres, showing the agreement of the experimental measurements (points) and the theoretical model including burst release (lines): the drug is assumed to be uniformly distributed in all the samples.

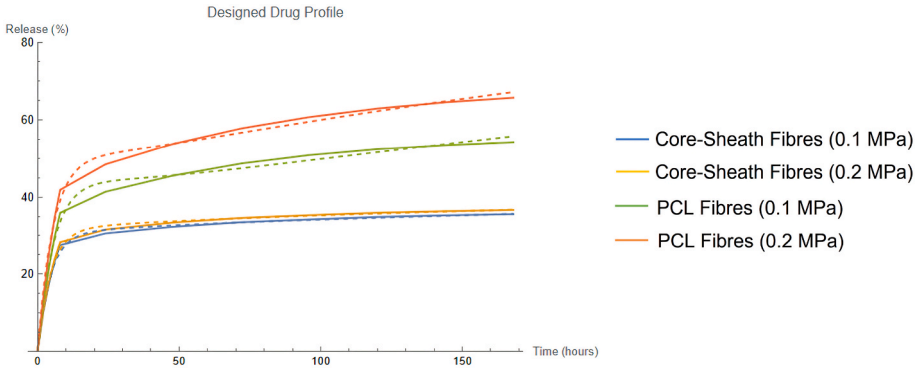

Fig. 12. The release percentage of TEHCL escaping from cylindrical fibres, showing the agreement of the experimental measurements (points) and the theoretical model including burst release (lines): this differs from Fig. 11 in that samples Core-Sheath 0.1 MPa and Core-Sheath 0.2 MPa use the core-sheath model.

Table 2
Values of diffusion coefficient D, burst release fraction and burst release rate constant k assuming a uniform drug concentration in all fibres. The uncertainties in D are caused by the uncertainties in the fibre diameters.

	Diameter μm	D m^2s^{-1}	f	ks^{-1}
Core-Sheath PCL:PVP (TEHCL) (0.1 MPa)	5.4 ± 1.4	$(2.0 \pm 0.5) \times 10^{-20}$	0.29	0.000062
Core-Sheath PCL:PVP (TEHCL) (0.2 MPa)	4.7 ± 1.4	$(1.6 \pm 0.5) \times 10^{-20}$	0.30	0.000061
PCL:TEHCL (0.1 MPa)	3.1 ± 1.1	$(1.14 \pm 0.33) \times 10^{-19}$	0.36	0.000056
PCL:TEHCL (0.2 MPa)	1.5 ± 0.3	$(4.2 \pm 0.8) \times 10^{-20}$	0.40	0.000057

Table 3
Values of diffusion coefficient D, burst release fraction and burst release rate constant k assuming the designed drug concentrations in all fibres. The uncertainties in D are caused by the uncertainties in the fibre diameters.

	Diameter μm	D m^2s^{-1}	f	ks^{-1}
Core-Sheath PCL:PVP (TEHCL) (0.1 MPa)	5.4 ± 1.4	$(2.0 \pm 0.5) \times 10^{-20}$	0.29	0.000062
Core-Sheath PCL:PVP (TEHCL) (0.2 MPa)	4.7 ± 1.4	$(1.6 \pm 0.5) \times 10^{-20}$	0.30	0.000061
PCL:TEHCL (0.1 MPa)	3.1 ± 1.1	$(3.3 \pm 0.9) \times 10^{-19}$	0.44	0.000049
PCL:TEHCL (0.2 MPa)	1.5 ± 0.3	$(7.9 \pm 1.6) \times 10^{-20}$	0.51	0.000051

confirmed the presence of both polymers in the core-sheath patches and that the drug was molecularly dispersed within the fibre matrix. Additionally, there was no interaction between the drug and polymer components in the fabricated fibres. Confocal microscopy analysis successfully confirmed the structure of the core-sheath fibre patches. The release profiles of antibacterial drug TEHCL over 168 h period in vitro were measured which demonstrated an initial burst release characteristic followed by a stable sustained release. The mathematical modelling of the experimental data confirmed that a burst release model fits the experiment better than a purely diffusive model. Core-sheath structures fabricated using this novel electric field free technique provides greater opportunities to encapsulate or coat numerous growth factors, drugs and peptides in a more precisely time-programmed manner; increasing access to mass-scale production and cost-effective treatment.

Author statement

All authors contributed to the writing and editing of the manuscript. **Hamta Majd** conducted the research and investigation process, performed the experiments and analysed the data. **Anthony Harker** applied statistical and mathematical models to analyse the data. **Mohan Edirisinghe** supervised and coordinated the research. **Maryam Parhizkar** supervised and managed the overall aspects of the research.

Declaration of competing interests

The authors declare that they have no known competing financial interests or personal relationships that could have appeared to influence the work reported in this paper.

References

[1] A. Friman, B. Klang, B. Ebbeskog, Wound care in primary health care: district nurses' needs for co-operation and well-functioning organization, J. Interprof. Care 24 (1) (2010) 90–99.
[2] S. Dhivya, V.V. Padma, E. Santhini, Wound dressings - a review, Biomed. Taiwan. 5 (4) (2015) 24–28.
[3] C. Shi, C. Wang, H. Liu, Q. Li, R. Li, Y. Zhang, et al., Selection of appropriate wound dressing for various wounds, Front. Bioeng. Biotechnol. 8 (2020) 182.
[4] G.C. Fowler, Pfenninger and Fowler's Procedures for Primary Care E-Book, Elsevier Health Sciences, 2019.
[5] J.C. Dumville, E.S. Petherick, S. O'Meara, P. Raynor, N. Cullum, How is research evidence used to support claims made in advertisements for wound care products? J. Clin. Nurs. 18 (10) (2009) 1422–1429.
[6] A. Knowles, 15 dressings: is there an evidence base? Foot Diabetes. 460 (2006) 186.
[7] L. Hussey, S.J. Stocks, P. Wilson, J.C. Dumville, N. Cullum, Use of antimicrobial dressings in England and the association with published clinical guidance: interrupted time series analysis, BMJ Open 9 (9) (2019), e028727.
[8] J.F. Guest, G.W. Fuller, P. Vowden, Cohort study evaluating the burden of wounds to the UK's National Health Service in 2017/2018: update from 2012/2013, BMJ Open 10 (12) (2020), e045253.
[9] D. Simões, S.P. Miguel, M.P. Ribeiro, P. Coutinho, A.G. Mendonça, I.J. Correia, Recent advances on antimicrobial wound dressing: a review, Eur. J. Pharm. Biopharm. 127 (2018) 130–141.
[10] V. Jones, J.E. Grey, K.G. Harding, Wound dressings, BMJ 332 (7544) (2006) 777–780.
[11] Z. Li, M. Knetsch, Antibacterial strategies for wound dressing: preventing infection and stimulating healing, Curr. Pharmaceut. Des. 24 (8) (2018) 936–951.
[12] L.G. Ovington, Advances in wound dressings, Clin. Dermatol. 25 (1) (2007) 33–38.
[13] T. Velnar, T. Bailey, V. Smrkolj, The wound healing process: an overview of the cellular and molecular mechanisms, J. Int. Med. Res. 37 (5) (2009) 1528–1542.
[14] S. Guo, L.A. DiPietro, Factors affecting wound healing, J. Dent. Res. 89 (3) (2010) 219–229.
[15] C. Thomas Hess, Checklist for factors affecting wound healing, Adv. Skin Wound Care 24 (4) (2011).
[16] C. Pathak, F.U. Vaidya, S.M. Pandey, Mechanism for development of nanobased drug delivery system, Appl. Targeted Nano. Deliv. Syst. (2019) 35–67.
[17] Kenry, C.T. Lim, Nanofiber technology: current status and emerging developments, Prog. Polym. Sci. 70 (2017) 1–17.
[18] B. Simionescu, D. Ivanov, Natural and synthetic polymers for designing composite materials, Handb. Bioceram. Biocomposites. (2016) 233–286.
[19] C. Wang, J. Wang, L. Zeng, Z. Qiao, X. Liu, H. Liu, et al., Fabrication of electrospun polymer nanofibers with diverse morphologies, Molecules 24 (5) (2019) 834.
[20] X. Xia, Y. Wang, A. Ruditskiy, Y. Xia, 25th Anniversary Article: galvanic replacement: a simple and versatile route to hollow nanostructures with tunable and well-controlled properties, Adv. Mater. 25 (44) (2013) 6313–6333.
[21] J.T. McCann, D. Li, Y. Xia, Electrospinning of nanofibers with core-sheath, hollow, or porous structures, J. Mater. Chem. 15 (7) (2005) 735–738.
[22] P. Gupta, G.L. Wilkes, Some investigations on the fiber formation by utilizing a side-by-side bicomponent electrospinning approach, Polymer 44 (20) (2003) 6353–6359.
[23] Q.P. Pham, U. Sharma, A.G. Mikos, Electrospun poly (ε-caprolactone) microfiber and multilayer nanofiber/microfiber scaffolds: characterization of scaffolds and measurement of cellular infiltration, Biomacromolecules 7 (10) (2006) 2796–2805.
[24] V. Leung, F. Ko, Biomedical applications of nanofibers, Polym. Adv. Technol. 22 (3) (2011) 350–365.
[25] Z.-M. Huang, Y.Z. Zhang, M. Kotaki, S. Ramakrishna, A review on polymer nanofibers by electrospinning and their applications in nanocomposites, Compos. Sci. Technol. 63 (15) (2003) 2223–2253.
[26] A. Ziabicki, Fundamentals of Fibre Formation : the Science of Fibre Spinning and Drawing, Wiley, London; New York, 1976.
[27] W. Xu, L. Xia, X-h Zhou, P. Xi, B-w Cheng, Y-x Liang, Hollow carbon microfibres fabricated using coaxial centrifugal spinning, Micro & Nano Lett. 11 (2) (2016) 74–76.
[28] A. Magaz, A.D. Roberts, S. Faraji, T.R.L. Nascimento, E.S. Medeiros, W. Zhang, et al., Porous, aligned, and biomimetic fibers of regenerated silk fibroin produced by solution blow spinning, Biomacromolecules 19 (12) (2018) 4542–4553.
[29] P.F. Ng, K.I. Lee, S. Meng, J. Zhang, Y. Wang, B. Fei, Wet spinning of silk fibroin-based core–sheath fibers, ACS Biomater. Sci. Eng. 5 (6) (2019) 3119–3130.
[30] D. Han, A.J. Steckl, Coaxial electrospinning formation of complex polymer fibers and their applications, Chem. Plus. Chem. 84 (10) (2019) 1453–1497.
[31] J. Hong, M. Yeo, G.H. Yang, G. Kim, Cell-electrospinning and its application for tissue engineering, Int. J. Mol. Sci. 20 (24) (2019) 6208.
[32] M. Doostmohammadi, H. Forootanfar, S. Ramakrishna, Regenerative medicine and drug delivery: progress via electrospun biomaterials, Mater. Sci. Eng. C 109 (2020), 110521.
[33] S.S. Sankar, K. Karthick, K. Sangeetha, A. Karmakar, S. Kundu, Transition-metal-Based zeolite imidazolate framework nanofibers via an electrospinning approach: a review, ACS Omega 5 (1) (2020) 57–67.
[34] S. Mahalingam, S. Homer-Vanniasinkam, M. Edirisinghe, Novel pressurised gyration device for making core-sheath polymer fibres, Mater. Des. 178 (2019), 107846.
[35] S. Mahalingam, S. Huo, S. Homer-Vanniasinkam, M. Edirisinghe, Generation of core–sheath polymer nanofibers by pressurised gyration, Polymers 12 (8) (2020).
[36] S. Mahalingam, C. Bayram, M. Gultekinoglu, K. Ulubayram, S. Homer-Vanniasinkam, M. Edirisinghe, Co-axial gyro-spinning of PCL/PVA/HA core-sheath fibrous scaffolds for bone tissue engineering, Macromol. Biosci. 21 (10) (2021), 2100177.
[37] S. Agarwal, J.H. Wendorff, A. Greiner, Use of electrospinning technique for biomedical applications, Polymer 49 (26) (2008) 5603–5621.
[38] X. Yan, J. Marini, R. Mulligan, A. Deleault, U. Sharma, M.P. Brenner, et al., Slit-surface electrospinning: a novel process developed for high-throughput fabrication of core-sheath fibers, PLoS One 10 (5) (2015), e0125407.
[39] S. Mahalingam, R. Matharu, S. Homer-Vanniasinkam, M. Edirisinghe, Current methodologies and approaches for the formation of core–sheath polymer fibers for biomedical applications, Appl. Phys. Rev. 7 (4) (2020), 041302.
[40] Y. Xin, Z. Huang, W. Li, Z. Jiang, Y. Tong, C. Wang, Core–sheath functional polymer nanofibers prepared by co-electrospinning, Eur. Polym. J. 44 (4) (2008) 1040–1045.
[41] Y. Pilehvar-Soltanahmadi, A. Akbarzadeh, N. Moazzez-Lalaklo, N. Zarghami, An update on clinical applications of electrospun nanofibers for skin bioengineering, Artif. Cell Nanomed. Biotechnol. 44 (6) (2016) 1350–1364.
[42] M. Naeimirad, A. Zadhoush, R. Kotek, R. Esmaeely Neisiany, S. Nouri Khorasani, S. Ramakrishna, Recent advances in core/shell bicomponent fibers and nanofibers: a review, J. Appl. Polym. Sci. 135 (21) (2018) 46265.
[43] M. Dasdemir, B. Maze, N. Anantharamaiah, B. Pourdeyhimi, Influence of polymer type, composition, and interface on the structural and mechanical properties of core/sheath type bicomponent nonwoven fibers, J. Mater. Sci. 47 (16) (2012) 5955–5969.
[44] S.-F. Chou, D. Carson, K.A. Woodrow, Current strategies for sustaining drug release from electrospun nanofibers, J. Contr. Release 220 (2015) 584–591.
[45] C.L. He, Z.M. Huang, X.J. Han, L. Liu, H.S. Zhang, L.S. Chen, Coaxial electrospun poly(L-lactic acid) ultrafine fibers for sustained drug delivery, J. Macromol. Sci., Part B. 45 (4) (2006) 515–524.
[46] V. Pillay, C. Dott, Y.E. Choonara, C. Tyagi, L. Tomar, P. Kumar, et al., A review of the effect of processing variables on the fabrication of electrospun nanofibers for drug delivery applications, 2013, J. Nanomater. (2013), 789289.
[47] B. Azimi, P. Nourpanah, M. Rabiee, S. Arbab, Poly J -caprolactone) fiber: an overview, J. Eng. Fibers and Fabrics. 9 (2014).
[48] E. Malikmammadov, T.E. Tanir, A. Kiziltay, V. Hasirci, N. Hasirci, PCL and PCL-based materials in biomedical applications, J. Biomater. Sci. Polym. Ed. 29 (7–9) (2018) 863–893.
[49] P. Franco, I. De Marco, The use of poly(N-vinyl pyrrolidone) in the delivery of drugs: a review, Polymers 12 (5) (2020) 1114.
[50] N. Garrido-Mesa, A. Zarzuelo, J. Gálvez, Minocycline: far beyond an antibiotic, Br. J. Pharmacol. 169 (2) (2013) 337–352.
[51] H. Ezhilarasu, R. Ramalingam, C. Dhand, R. Lakshminarayanan, A. Sadiq, C. Gandhimathi, et al., Biocompatible aloe vera and tetracycline hydrochloride loaded hybrid nanofibrous scaffolds for skin tissue engineering, Int. J. Mol. Sci. 20 (20) (2019) 5174.
[52] J. Crank, The Mathematics of Diffusion, Oxford university press, 1979.
[53] P. Zahedi, I. Rezaeian, S.H. Jafari, Z. Karami, Preparation and release properties of electrospun poly(vinyl alcohol)/poly(E >-caprolactone) hybrid nanofibers: optimization of process parameters via D-optimal design method, Macromol. Res. 21 (2012).
[54] U.E. Illangakoon, S. Mahalingam, R.K. Matharu, M. Edirisinghe, Evolution of surface nanopores in pressurised gyrospun polymeric microfibers, Polymers 9 (10) (2017).
[55] J.M. Deitzel, J. Kleinmeyer, D. Harris, N.C. Beck Tan, The effect of processing variables on the morphology of electrospun nanofibers and textiles, Polymer 42 (1) (2001) 261–272.
[56] H. Li, G.R. Williams, J. Wu, H. Wang, X. Sun, L.-M. Zhu, Poly (N-isopropylacrylamide)/poly (l-lactic acid-co-ε-caprolactone) fibers loaded with ciprofloxacin as wound dressing materials, Mater. Sci. Eng. C 79 (2017) 245–254.
[57] G.A. Kannon, A.B. Garrett, Moist wound healing with occlusive dressings, Dermatol. Surg. 21 (7) (1995) 583–590.
[58] J. Wu, Z. Zhang, Jg Gu, W. Zhou, X. Liang, G. Zhou, et al., Mechanism of a long-term controlled drug release system based on simple blended electrospun fibers, J. Contr. Release 320 (2020) 337–346.
[59] Kamaruddin, D. Edikresnha, I. Sriyanti, M.M. Munir, Khairurrijal, Synthesis of polyvinylpyrrolidone (PVP)-Green tea extract composite nanostructures using electrohydrodynamic spraying technique, IOP Conf. Ser. Mater. Sci. Eng. 202 (2017), 012043.
[60] A. Rahma, M.M. Munir, Khairurrijal, A. Prasetyo, V. Suendo, H. Rachmawati, Intermolecular interactions and the release pattern of electrospun curcumin-polyvinyl(pyrrolidone) fiber, Biol. Pharm. Bull. 39 (2) (2016) 163–173.
[61] Y. Gao, M.W. Chang, Z. Ahmad, J.S. Li, Magnetic-responsive microparticles with customized porosity for drug delivery, RSC Adv. 6 (91) (2016) 88157–88167.
[62] A. Caroni, C. De Lima, M. Pereira, J. Fonseca, Tetracycline adsorption on chitosan: a mechanistic description based on mass uptake and zeta potential measurements, Colloids Surf. B Biointerfaces 100 (2012) 222–228.
[63] E. Abdelrazek, A. Abdelghany, S. Badr, M. Morsi, Morphological, thermal and electrical properties of (PEO/PVP)/Au nanocomposite before and after gamma-irradiation, J. Res. Updates Polym. Sci. 6 (2) (2017) 45–54.
[64] L. Wang, C.C. Zhang, H.M.D. Wang, Z. Ahmad, J.S. Li, M.W. Chang, High throughput engineering and use of multi-fiber composite matrices for controlled active release, Mater. Today Commun. 17 (2018) 53–59.
[65] X.M. Zeng, G.P. Martin, C. Marriott, Effects of molecular weight of polyvinylpyrrolidone on the glass transition and crystallization of co-lyophilized sucrose, Int. J. Pharm. 218 (1–2) (2001) 63–73.

[66] C.U. Turan, A. Metin, Y. Guvenilir, Controlled release of tetracycline hydrochloride from poly (ω-pentadecalactone-co-ε-caprolactone)/gelatin nanofibers, Eur. J. Pharm. Biopharm. 162 (2021) 59–69.
[67] S. Govender, V. Pillay, D. Chetty, S. Essack, C. Dangor, T. Govender, Optimisation and characterisation of bioadhesive controlled release tetracycline microspheres, Int. J. Pharm. 306 (1–2) (2005) 24–40.
[68] Y.N. Jiang, H.Y. Mo, D.G. Yu, Electrospun drug-loaded core-sheath PVP/zein nanofibers for biphasic drug release, Int. J. Pharm. 438 (1–2) (2012) 232–239.
[69] D.G. Yu, X. Wang, X.Y. Li, W. Chian, Y. Li, Y.Z. Liao, Electrospun biphasic drug release polyvinylpyrrolidone/ethyl cellulose core/sheath nanofibers, Acta Biomater. 9 (3) (2013) 5665–5672.
[70] Z. Li, H. Kang, N. Che, Z. Liu, P. Li, W. Li, et al., Controlled release of liposome-encapsulated Naproxen from core-sheath electrospun nanofibers, Carbohydr. Polym. 111 (2014) 18–24.
[71] Q.L. Loh, C. Choong, Three-dimensional scaffolds for tissue engineering applications: role of porosity and pore size, Tissue Eng. B Rev. 19 (6) (2013) 485–502.